On quantification errors of R_2^* and proton density fat fraction mapping in trabecularized bone marrow in the static dephasing regime

Sophia Kronthaler[1] | **Maximilian N. Diefenbach[1]** | **Christof Boehm[1]** |
Mark Zamskiy[1] | **Marcus R. Makowski[1]** | **Thomas Baum[2]** |
Nico Sollmann[2,3,4] | **Dimitrios C. Karampinos[1]**

[1]Department of Diagnostic and Interventional Radiology, School of Medicine, Klinikum rechts der Isar, Technical University of Munich, Munich, Germany

[2]Department of Diagnostic and Interventional Neuroradiology, School of Medicine, Klinikum rechts der Isar, Technical University of Munich, Munich, Germany

[3]TUM-Neuroimaging Center, Klinikum rechts der Isar, Technical University of Munich, Munich, Germany

[4]Department of Diagnostic and Interventional Radiology, University Hospital Ulm, Ulm, Germany

Correspondence
Sophia Kronthaler, Department of Diagnostic and Interventional Radiology, Klinikum rechts der Isar, Technische Universität München, Ismaninger Str. 22, 81675 Munich, Germany.
Email: sophia.kronthaler@tum.de

Purpose: To study the effect of field inhomogeneity distributions in trabecularized bone regions on the gradient echo (GRE) signal with short TEs and to characterize quantification errors on R_2^* and proton density fat fraction (PDFF) maps when using a water-fat model with an exponential R_2^* decay model at short TEs.

Methods: Field distortions were simulated based on a trabecular bone micro CT dataset. Simulations were performed for different bone volume fractions (BV/TV) and for different bone-fat composition values. A multi-TE UTE acquisition was developed to acquire multiple UTEs with random order to minimize eddy currents. The acquisition was validated in phantoms and applied in vivo in a volunteer's ankle and knee. Chemical shift encoded MRI (CSE-MRI) based on a Cartesian multi-TE GRE scan was acquired in the spine of patients with metastatic bone disease.

Results: Simulations showed that signal deviations from the exponential signal decay at short TEs were more prominent for a higher BV/TV. UTE multi-TE measurements reproduced in vivo the simulation-based predicted behavior. In regions with high BV/TV, the presence of field inhomogeneities induced an R_2^* underestimation in trabecularized bone marrow when using CSE-MRI at 3T with a short TE.

Conclusion: R_2^* can be underestimated when using short TEs (<2 ms at 3 T) and a water-fat model with an exponential R_2^* decay model in multi-echo GRE acquisitions of trabecularized bone marrow.

KEYWORDS
chemical shift encoding (CSE), Gaussian decay, magnetically inhomogeneous tissues, PDFF mapping, R_2^* mapping, signal decay, static dephasing regime, trabecularized bone, ultra-short echo time (UTE)

1 | INTRODUCTION

The clinical need for early diagnosis of osteoporosis, for assessment of fracture risk, and for therapy response monitoring has been driving the development of MRI methods to assess trabecular bone density and microstructure in vivo.[1-3] Trabecular bone consists of a complex network of bone tissue, which can comprise around 30% of the total tissue volume. The trabecular bone cavities are filled with fatty bone marrow.[4] Since bone signal decays rapidly with a very short T_2^*, in conventional MRI methods the signal of bone marrow was used indirectly to assess trabecular bone. First, high-resolution imaging was used to resolve the trabecular bone matrix as signal void within the bone marrow signal. However, high-resolution MR trabecular bone imaging is limited to distal skeletal sites and due to its low sensitivity and motion.[2,5] Beyond high-resolution trabecular bone imaging, trabecular bone has been typically indirectly evaluated by measurements of effective bone marrow properties. T_2^* and R_2^* measurements in trabecularized bone marrow have been correlated with the bone mineral density since early works[5-9] and R_2^* has been proposed as a biomarker for bone loss in osteoporosis.[1,10-12] More recently the proton density fat fraction (PDFF) has been introduced as a biomarker of bone marrow fat content changes associated with bone loss.[1,2,12-14] Therefore, chemical shift encoding-based (CSE) water-fat separation assuming a single R_2^* exponential signal decay has been proposed to simultaneously assess changes in the trabecular bone matrix by R_2^* quantification and in bone marrow fat content by PDFF quantification.[1,2,13,15]

The trabecular bone network presents an inherently complex topology with the bony trabeculae and the signal generating bone marrow in the intra-trabecular space. The susceptibility difference between bone and marrow and the underlying complex microstructure cause a large distribution of inhomogeneities of the induced magnetic field within each voxel. Due to the distribution of field inhomogeneities, spins dephase rapidly and consequently yield a decreased TR due to intravoxel dephasing. It was shown previously, in simulations[16,17] and in theoretical analyses,[18,19] that, in the static dephasing regime, the intra-voxel dephasing can be described as a mono-exponential decay with decay rate R_2^*. The static dephasing regime applies if diffusion effects become negligible as the dephasing field inhomogeneities are much stronger than the signal decay due to diffusive motion. The exponential decay originates from the assumption of Lorentzian distribution of field inhomogeneities. The frequency spectrum of an FID has a Lorentzian line shape with the FWHM of the Lorentzian distribution being equal to $\frac{R_2^*}{\pi}$.[20] In the static dephasing regime and within trabecular bone, it was shown that R_2^* depends on the bone density as well as the orientation

of trabecular bone with respect to the main magnetic field.[7,9,18,21]

The above described mono-exponential signal decay behavior, however, applies only for long TEs. In reality and for large field inhomogeneities, the distribution is not necessarily Lorentzian and resembles a Gaussian shape, which will affect the decay behavior for short TEs.[18,19,22] Therefore, at short TEs there are two effects that need to be considered. There is additional signal from short T_2^* tissue such as the bone matrix and, due to the underlying microstructure, the surrounding bone marrow signal follows a Gaussian decay. The characteristic TE, that defines the time point at which the Gaussian decay deviates from the mono-exponential decay, may be of the order of the shortest achievable TEs that are commonly used at CSE-MRI acquisitions of bone marrow.[18,19,23,24] In CSE-MRI, a typical acquisition strategy aims to minimize the first TE to increase the SNR, and water-fat signal modeling typically relies on the assumption of a mono-exponential single R_2^* signal decay. The question of the influence of large field inhomogeneities on the R_2^* signal decay at short TEs has not been addressed before and needs the ability to measure the decaying signal at UTE. Therefore, the purpose of this work is to investigate, with the help of a UTE acquisition, the quantification errors of R_2^* and PDFF maps in trabecularized bone marrow regions in the static dephasing regime when using a water-fat model with an exponential R_2^* decay model at short TEs.

2 | METHODS

2.1 | Bone cubes forward simulation

Similar to previous work on simulating magnetic fields, magnetic field offsets caused by a trabecular bone model were simulated.[9,16,17] Therefore, a micro computed tomography (CT) dataset was acquired with 45.6 μm isotropic resolution of a healthy human femur bone cube with a size of $180 \times 180 \times 180$ mm^3, containing only trabecular bone structure. From the micro-CT images, a bone mask was derived by applying a simple threshold at 50% (Figure 1A). The bone volume to total volume (BV/TV) ratio of each femoral cube was estimated by taking the mean inside the bounding box of the binary mask. A susceptibility map was obtained by assigning the susceptibility χ of bone and marrow to the bone mask with $\Delta\chi$ being defined as the difference between bone matrix to the surrounding marrow. According to the forward model as described earlier,[25,26] the relative distance field (RDF), deviations from the applied magnetic field, was simulated with one fixed B_0-direction, with varying $\Delta\chi$ and with varying BV/TV ratios. The BV/TV ratio of the bone masks was

(A)

(B)

(C)

(D)
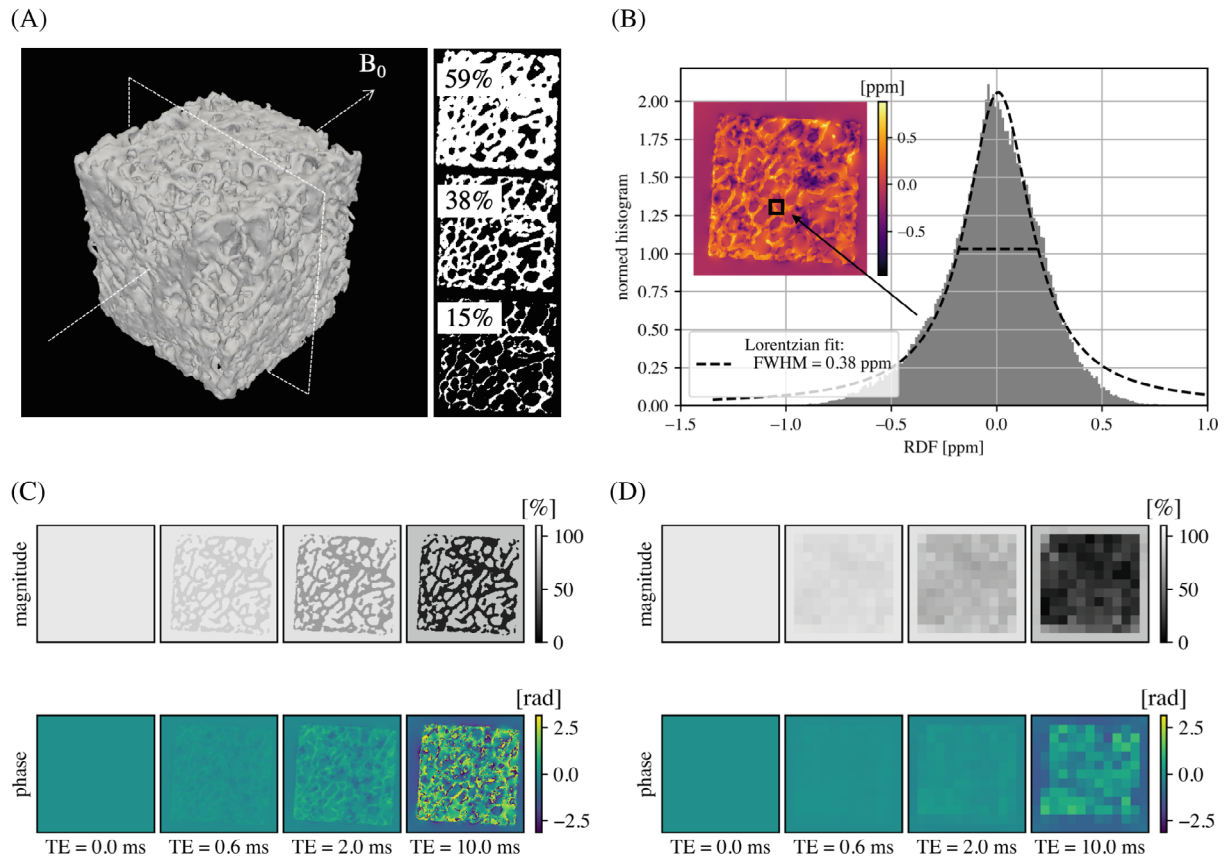
FIGURE 1 Illustration of the bone cube simulations. A, A bone mask was generated from a microscopic CT scan of resolution 45.6 μm (BV/TV 38%). B, The BV/TV was altered by erosion (BV/TV = 15%) and dilation (BV/TV = 59%). Forward simulated relative field map. The black square shows the size of a 1.5×1.5 mm² MR voxel and the distribution of the relative difference field (RDF) within the MR voxel. The FWHM of a Lorentzian fit was calculated to give an estimate of the signal decay due to the distribution of local inhomogeneities. With the field-map a signal for different TEs is generated on the microscopic CT scale (C) and down-sampled to the MR resolution of 1.5×1.5 mm² (D). RDF: relative distance field

altered by erosion and dilation with standard image processing tools (Python version 3.9.0, binary erosion/dilation from the ndimage scipy module with a nearest neighbor kernel, SciPy Version 1.7.1) to simulate the degeneration of trabecular bone comparable to the degeneration of bone in osteoporosis (Figure 1A). An auto-binned (Freedman Diaconis Estimator) histogram of all field values outside the trabecular bone was generated and shows the distribution of local field inhomogeneities within a $1.5 \text{ mm} \times 1.5 \text{ mm} \times 1.5 \text{ mm}$ voxel (Figure 1B). The FWHM of the fitted Lorentzian curve was calculated to give an estimate of the reversible relaxation rate R_2'. The resulting RDF map was used to simulate a complex multi-echo signal at 3 T with TE = 0–10 ms and ΔTE = 0.2 ms (Figure 1C), assuming the following single- R_2^* bone signal model and single- R_2^* multi-fat-peak fat signal model.

$$S(t) = \begin{cases} \rho e^{-R_{2,B}^* t} & \text{in the bone matrix} \\ c(t)\, e^{-R_{2,F} t} e^{i2\pi f_{RDF}\, t} & \text{in the bone marrow} \end{cases}$$

$$\text{with } c(t) = \sum_{p=1}^{P} \alpha_p e^{i2\pi \Delta f_p t} \tag{1}$$

The fat signal was modeled by an a priori known spectrum $c(t)$ with P spectral peaks with relative amplitudes α_p and chemical shift Δf_p. The bone signal was modeled with a simple mono-exponential decay with ρ as the density of the bone matrix normalized by the density of the bone marrow. The simulated signal on the microscopic scale was down-sampled to the MR-like isotropic resolution of 1.5 mm by averaging the signal (Figure 1D). To assess the effect of local field inhomogeneities on the signal decay, caused by the susceptibility difference between bone and marrow, bone cube simulations with varying BV/TV ratios were performed (Figure 2A,B). Furthermore, the simulations were repeated for different signal models and a fixed BV/TV of 38% (Figure 2C,D): a) without bone matrix signal $\rho = 0$ and with a single-fat-peak fat model $T_{2,F} = 60$ ms,[27,28] $c(t) = 1$ b) without bone matrix signal ($\rho = 0$) and with a nine-peak marrow fat spectrum model[29]
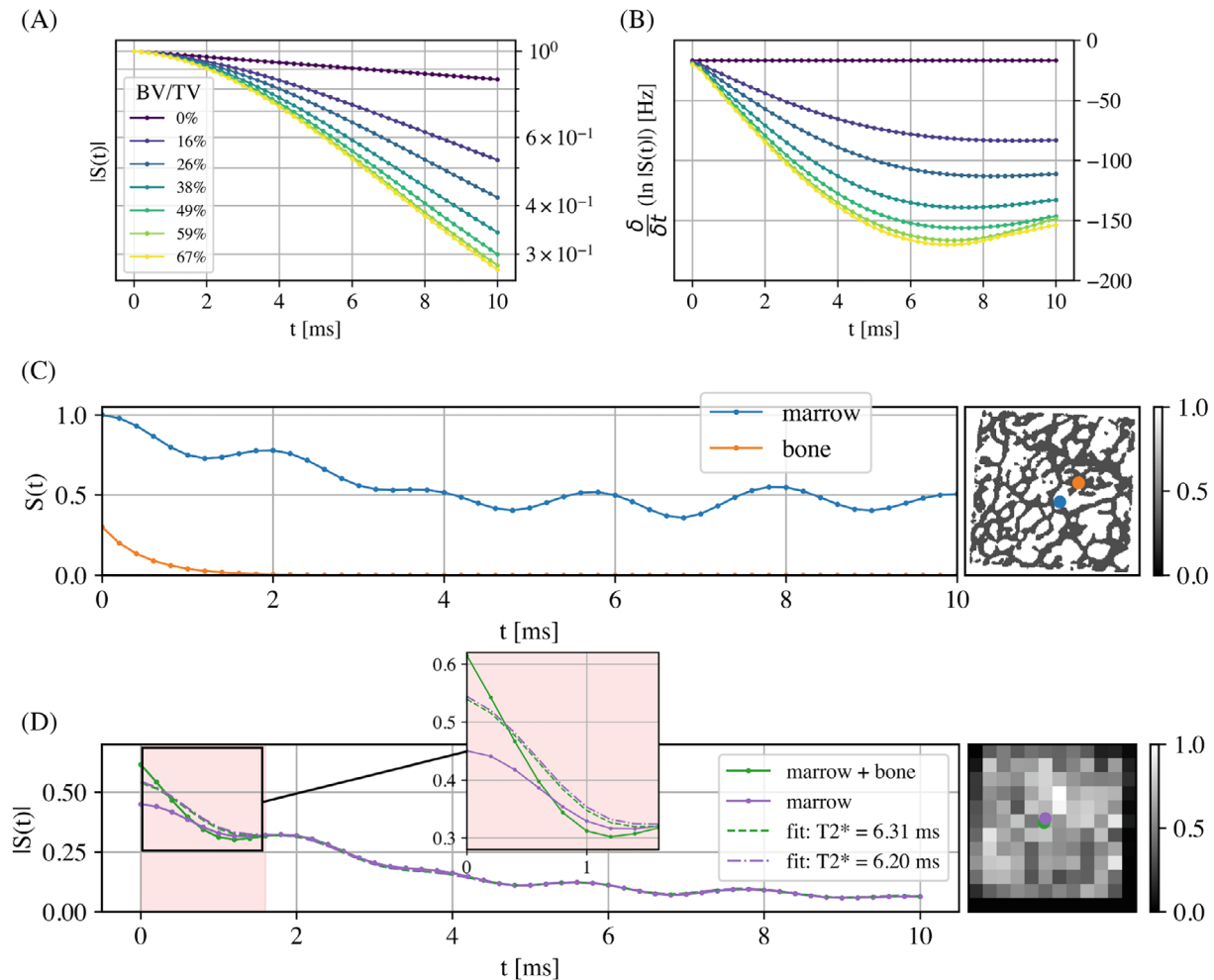
FIGURE 2 Simulation results. A, Simulation of the macroscopic signal for varying BV/TV. Only the marrow signal was included in the simulation ($\rho = 0$) with a single-fat-peak fat model ($c(t) = 1$). For a BV/TV of 0%, the signal followed a mono-exponential decay with $T_{2,F} = 60$ ms. B, The corresponding signal derivative shows that for a non-zero BV/TV the local distribution of RDFs yielded a Gaussian decay at low TEs and an exponential decay at larger TEs. C, Simulation of the microscopic signal for a voxel containing only bone and for a voxel containing only marrow. The bone signal followed a mono-exponential decay with $T_{2,B}^* = 0.5$ ms. The marrow signal showed oscillations due to the nine-peak marrow fat spectrum. D, Simulation of the macroscopic signal including either only the signal of marrow or including the signal of both bone and marrow. The dashed lines show fitting results when only data points at TEs larger than 2 ms were included. The extrapolation of the fit at TEs <2 ms resulted in a higher signal when compared to the simulation result (red area)

($T_{2,F} = 60$ ms) and c) with bone matrix signal[30] ($\rho = 0.3$, $T_{2,B}^* = 0.5$ ms) and with a nine-peak marrow fat spectrum model[29] ($T_{2,F} = 60$ ms).

2.2 | Multi-TE UTE pulse sequence

To measure the signal at short TEs, a 3D UTE stack-of-stars center-out radial sequence was employed[31] (Figure 3A). The non-selective RF excitation pulse was followed by a short phase-encoding gradient that adds a Cartesian dimension along the slice encoding direction. The duration of the phase-encoding gradient varied depending on the slice encoding. In addition, a variable delay dTE was

added, between the excitation pulse and slice encoding gradient, to achieve an arbitrary TE.[32] The delay was modified between TRs in a random order to prevent potential eddy current artifacts as described in[32] (Figure 3B). All TEs along one spoke were acquired first, before the acquisition of the next spoke. All spokes within one slice were acquired with a uniform, constant azimuthal angle sampling pattern. The minimal FID readout time of 0.14 ms was defined by the RF transmit–receive switching time of the system. A minimum TE of 0.19 ms was used for all measurements to give the coil system more time to tune the receive coil and eliminate remaining switching transients. All images were acquired on a 3T system (Elition X, Release 5.4; Philips Medical Systems).
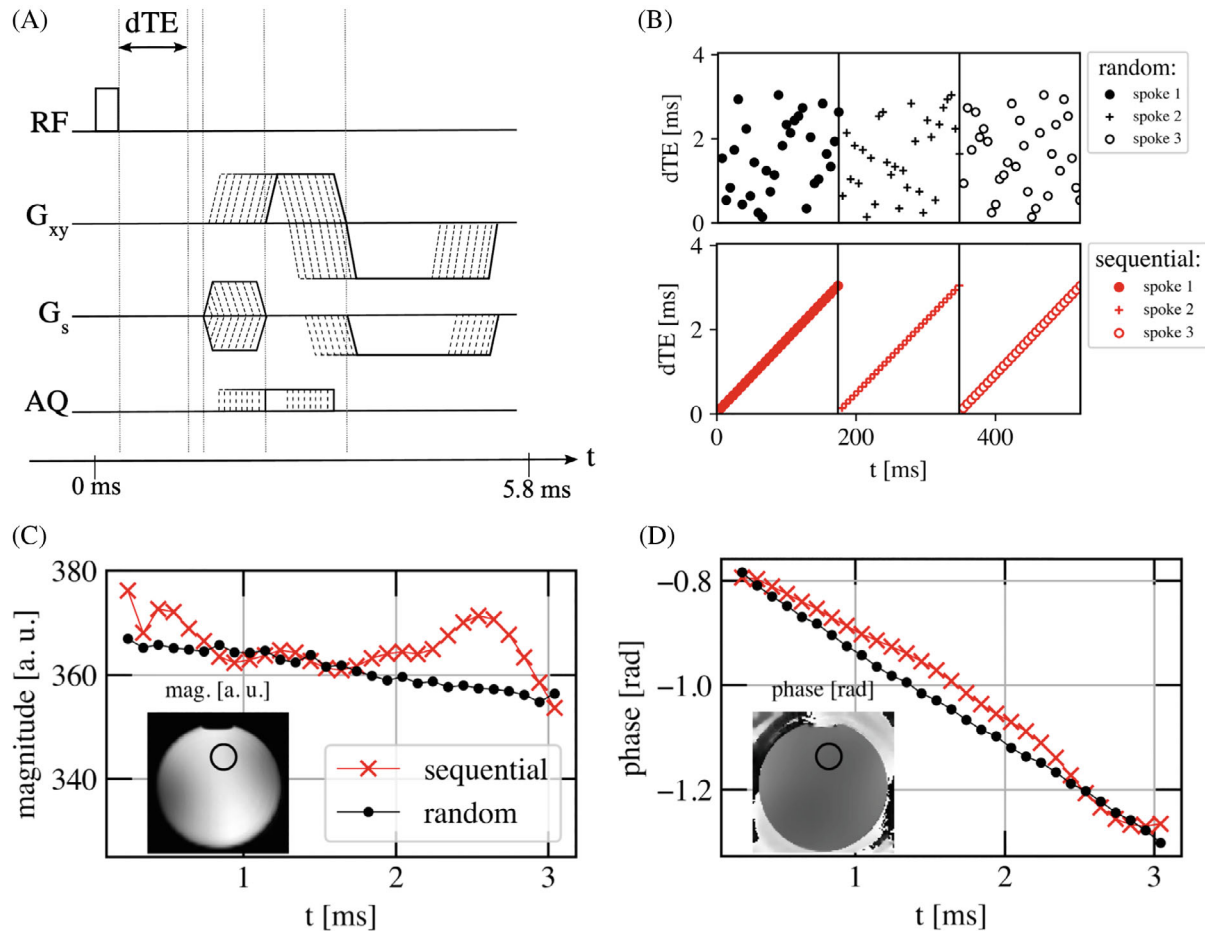
FIGURE 3 3D multi-TE UTE stack-of-stars acquisition: A, After the non-selective excitation, the FID readout started after a variable delay *dTE*. B, All TEs along one spoke were acquired in random order and before the readout of the next spoke. For comparison, the same acquisition was repeated with a sequential ordering of the TEs. C, D, Magnitude and phase over time of a phantom filled with water for the random (black) and the sequential (red) acquisition scheme

2.3 | Phantom measurements

To validate the signal stability of the multi-TE UTE acquisition strategy used, phantom measurements were performed in a water phantom and in water-fat phantoms with PDFF values of 0%, 5%, 15% and 100%.

For the measurement of the signal decay curves in the water phantom, an extensive coronal echo multi-TE UTE sampling was performed with 29 TEs in the range from 0.19 ms to 2.9 ms (Figure 1C, D) and the following scan parameters: TR 5.8 ms, flip angle (FA) 5°, in-plane resolution 1.5×1.5 mm^2, slice thickness 3 mm, FOV $180 \times 180 \times 116$ mm^3, receiver bandwidth 1440 Hz/pixel, and scan time of 16.4 min.

For the measurements of the PDFF phantoms a multi-TE UTE axial scan with 15 TEs was acquired with the following scan parameters: TE = [0.19, 0.24, 0.34, 0.44, 0.54, 0.64, 0.74, 0.84, 0.94, 1.04 1.14, 2.24, 3.34, 4.44, 5.54, 6.64] ms, TR 9.2 ms, FA 5°, in-plane

resolution 1.5×1.5 mm^2, slice thickness 5 mm, FOV $100 \times 100 \times 250$ mm^3, receiver bandwidth 1426 Hz/pixel and scan time of 11.7 min.

For conventional Dixon imaging and for comparison, a 3D Cartesian six-echo monopolar time-interleaved multi-echo gradient-echo (GRE) sequence was used as described previously[33] with the following parameters: two interleaves with three echoes per TR and TR/TE$_1$/ΔTE: 7.7/1.25/1.1 ms, FA 3°, voxel size $1.5 \times 1.5 \times 5$ mm^3, FOV $100 \times 100 \times 250$ mm^3, receiver bandwidth 1213 Hz/pixel, frequency direction anterior–posterior, scan time: 3.7 min.

2.4 | In vivo measurements

In vivo imaging was performed in the ankle and the knee of a healthy volunteer. Furthermore, clinical routine MR image data of the lumbar spine in three patients were retrospectively analyzed. The in vivo study part was approved

by the local institutional review board (Klinikum rechts der Isar, Technical University of Munich, Munich, Germany).

For the ankle measurements, a sagittal 3D multi-TE UTE measurement was performed with seven TEs, with a 16-channel ankle coil and the following parameters: TEs = [0.19 1.29 2.39 3.49 4.59 5.69 6.79] ms, FA 5°, FOV $220 \times 220 \times 90 \text{ mm}^3$, voxel size $1.2 \times 1.2 \times 3 \text{ mm}^3$, TR 3.4 ms, scan time 9.2 min, using a SENSE acceleration factor of 2 in the Cartesian-sampled dimension. Additionally, a Cartesian high-resolution balanced SSFP (bSSFP) reference scan was acquired with two phase cycles, TE 2.6 ms, FOV $220 \times 220 \times 90 \text{ mm}^3$, voxel size $0.3 \times 0.3 \times 1.5 \text{ mm}^3$.

For the knee measurements, a sagittal 3D multi-TE UTE measurement was performed with seven TEs, with a 16-channel transmit-receive knee coil and the following parameters: TE = [0.19 1.29 2.39 3.49 4.59 5.69 6.79] ms, FA 5°, FOV $130 \times 130 \times 105 \text{ mm}^3$, voxel size $1.48 \times 1.48 \times 2 \text{ mm}^3$, TR 10.1 ms, scan time 15.3 min, using a SENSE acceleration factor of 2 in the Cartesian-sampled dimension. Additionally, a Cartesian high-resolution bSSFP reference scan was acquired with two phase cycles, TE 2.6 ms, FOV $140 \times 140 \times 105 \text{ mm}^3$, and voxel size $0.45 \times 0.45 \times 2 \text{ mm}^3$.

For the calcaneus measurements, a sagittal Cartesian monopolar time-interleaved multi-echo gradient echo sequence was performed in three healthy volunteers. Scan parameters were: nine echoes in three acquisitions (three echoes per acquisition), $TE_1/\Delta TE$: 1.25/0.7 ms, readout direction feet-head, TR 13 ms, FA 5°, bandwidth/pixel = 1431.4 Hz, FOV $220 \times 220 \times 102 \text{ mm}^3$ and an isotropic voxel size of 1.5 mm. Additionally, all volunteer scans included a bSSFP sequence with two phase cycles, TE 3.4 ms, FOV $220 \times 220 \times 60 \text{ mm}^3$, voxel size $0.3 \times 0.3 \times 0.9 \text{ mm}^3$.

For the spine measurement, a sagittal Cartesian monopolar time-interleaved multi-echo gradient echo sequence was performed in the thoracolumbar spine of three patients where clinical MRI of the spine was performed either to assess degenerative disease or bone metastases. Subject 1: male, age 77, diagnosed with prostate cancer showed metastasis in L3 and extraosseous components. Subject 2: female, age 80, diagnosed with breast cancer showed diffuse metastases. Subject 3 male, age: 71, diagnosed with prostate cancer showed diffuse metastases. Scan parameters were: six echoes in two acquisitions (three echoes per acquisition), $TE_1/\Delta TE$: 1.12/0.96 ms, readout direction anterior–posterior, TR 8.3 ms, FA 5°, FOV $219.6 \times 219.6 \times 79.2 \text{ mm}^3$, and an isotropic voxel size of 1.8 mm. A CT scan was acquired within 30 days before the MRI for clinical purposes and was evaluated for osteoblastic metastatic lesions using

consensus reading (two neuroradiologists with >5 y of experience).

2.5 | Reconstruction and postprocessing

For the reconstruction of the UTE images, an image reconstruction toolbox (ReconFrame) was used to grid the UTE data in two dimensions with the corresponding k-space trajectories, to Fourier transform in 3D, and to perform SENSE unfolding in the third Cartesian-sampled dimension. The UTE k-space trajectories were corrected by means of a gradient impulse response function.[34]

All water–fat maps were calculated using CSE-based water-fat separation assuming the widely used single-R_2^* multi-fat-peak water-fat signal model,[35,36] tuned specifically to bone marrow.[29,37]

$$S(t) = \left(\rho_w + c(t)\rho_f \right) \; e^{-R_2^* t} e^{i2\pi f_B t} \tag{2}$$

with ρ_w and ρ_f the complex signal of water and fat components assuming an equal transverse relaxation rate R_2^* of water and fat, $c(t)$ the chemical shift components due to the multi-peak fat spectrum as described in Equation (1) and f_B the field map.

Given the small flip angles in all measurements, minimal T1 weighting was assumed and T1 bias was neglected.[38,39]

In a first step, the field map was calculated based on all TEs and with a robust graph-cut field-mapping method with a variable-layer construction[40] and based on the signal model introduced in Equation (2). The field map was used as initialization for all subsequent CSE-based processing.

In a second step, CSE-based water-fat separation was performed[37] again with the signal model in Equation (2) and with the field map result obtained in the first step. The parameter estimation problem was iteratively solved via alternating Gauss-Newton updates of the linear and nonlinear parameters in a variable projection method (VARPRO).[41] The CSE-based water-fat separation was performed once including all TEs and once including only later TEs. Plotted fitted signal magnitude curves were calculated based on the fitting parameters of the CSE processing.

3 | RESULTS

3.1 | Bone cube simulations

Figure 2A shows the simulation result of the macroscopic MR signal, which only included signal from the fatty bone

marrow ($\rho = 0$) with a single-fat-peak fat model ($c(t) = 1$). For a BV/TV ratio of 0%, meaning no bone was present in the marrow and no local field inhomogeneities, the signal followed a mono-exponential decay with $T_{2,F} = 60$ ms, which was the initial simulation parameter for the marrow relaxation rate. With an increase in BV/TV, two observations were made: (1) for TEs >6 ms the signal followed an exponential decay with a $T_{2,F}^* < 60$ ms and (2) for TEs <6 ms the signal followed a Gaussian decay. The change in the signal decay is highlighted with the derivative of the logarithm of the signal (Figure 2B). For longer TEs, the curve converged toward a constant value. For shorter TEs, the derivative followed a straight line.

Figure 2C shows the extension of the bone cube simulations when a nine-peak marrow fat spectrum and bone signal was added. In the microscopic picture, the signal for a voxel containing only bone followed a mono-exponential decay with $T_{2,B}^* = 0.5$ ms. The signal for a voxel containing only marrow showed a mono-exponential decay with $T_{2,F} = 60$ ms and with oscillations due to the nine-peak marrow fat spectrum. Using only the marrow signal from Figure 2C to generate the down-sampled macroscopic image (Figure 2D) resulted in a lower $T_2^* = 6.18$ ms when compared to the microscopic marrow signal. The extrapolation of the fit at TEs <2 ms resulted in a higher signal when compared to the simulation result. Including bone signal with $T_{2,B}^* = 0.5$ ms in the simulation yielded a $T_2^* = 6.28$ ms. The behavior of the signal curve was very similar to the signal including only marrow for TE >2 ms. Consequently, the difference between the fitted curves, including either only marrow or including bone and marrow, was small. For TE <1 ms, the additional signal of bone resulted in a higher signal amplitude compared to the marrow-only signal decay curve. In the area between 1 ms and 2 ms, the fit resulted in an overestimation of the simulated signal.

3.2 | Phantom measurements

The signal decay curves in the water phantom using the multi-TE UTE acquisition strategy showed a mono-exponential decay of the magnitude (Figure 3C) and a linear decrease of the phase (Figure 3D) when the random acquisition scheme was used. In comparison, the signal decay curve acquired with a sequential ordered, suffered from eddy current artifacts. Specifically, the magnitude showed signal fluctuations and a non-exponential decay behavior. The PDFF evaluation using the multi-TE UTE acquisition in comparison with a conventional Cartesian CSE-MRI acquisition showed a good agreement. Both PDFFs, acquired with the UTE acquisition and with the Cartesian acquisition, deviated slightly from the actual

PDFF values of 0%, 5%, 15%, and 100%. The PDFF values measured with the cartesian multi-echo sequence were 1.3%, 6.7%, 16.3%, and 100%, respectively. The PDFF values measured with the multi-TE UTE sequence were −3.1%, 3.7%, 16.1%, and 98.1%. For the Cartesian acquisition, the mean absolute error was 1.1% and for the UTE acquisition 1.9%.

3.3 | Multi-TE UTE in vivo measurements

To compare the signal decay at short TEs for different BV/TV ratios in vivo, a multi-TE UTE scan was performed in a healthy volunteer's ankle (Figure 4). The mean signal decay is shown for four selected regions of interest (ROIs). A Cartesian high-resolution bSSFP scan is shown as a reference and as an indicator for bone density. In the bSSFP scan, trabecular bone is only visible indirectly as the bone marrow presents strong MR signal and trabecular density is indicated by denser black signal drop out regions like in the subtalar. In regions with fewer trabeculae, bone marrow fills more volume and, consequently, MR signal is brighter as observed in the tuber calcanei. ROI 1 was placed within the cavum calcanei and showed a higher signal intensity in the bSSFP scan, higher fat content, compared to the other ROIs. ROI 2 was placed in the subtalar and showed the lowest signal intensity, higher BV/TV, compared to the other ROIs. The remaining ROIs (ROIs 3 and 4) were placed in the tuber calcanei and showed a higher signal intensity than ROI 1 and a lower signal intensity than ROI 4. In ROI 1, lower BV/TV ratios, the difference between the 7TEs fit and the 5TEs fit was small. For increasing BV/TV ratio, ROI 3 and 4, the difference at lower TEs increased as well. The largest difference was observed for ROI 2 with the largest BV/TV ratio. A voxel-wise comparison of the difference between the fits including all seven TEs or only the last five TEs is shown in Figure 5 by subtracting the two PDFF maps and the two R_2^* maps. The R_2^* difference maps showed a larger difference of 20% in R_2^* values for regions with higher bone densities such as the subtalar. The PDFF difference maps showed a small difference (5%) within the subtalar. Similar results were obtained in a healthy volunteer's knee (Figure 6), where the R_2^* differed in areas with higher bone density between fits over all TEs and fits over later TEs.

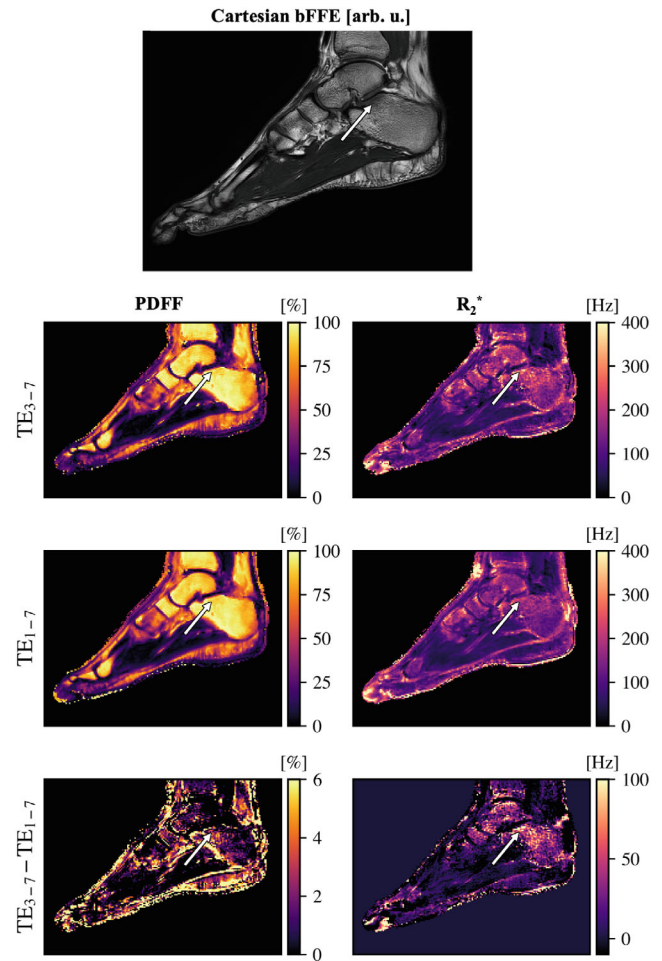## 3.4 | Cartesian multi-GRE in vivo measurements

Figure 7 shows a comparison of R_2^* maps obtained with a Cartesian multi-GRE scan in the calcaneus of three
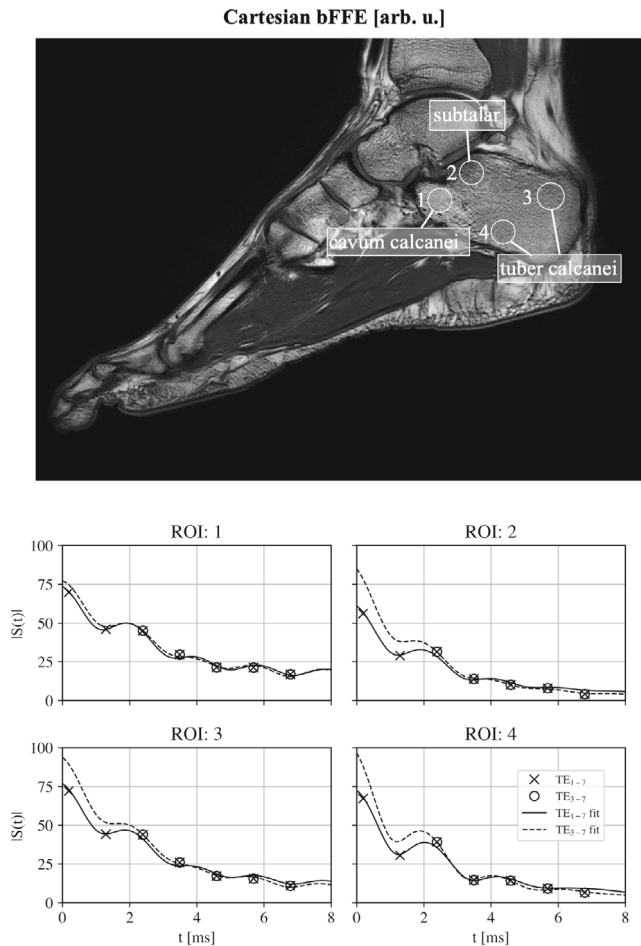
FIGURE 4 Signal decay curves of a multi-TE UTE acquisition of the calcaneus. The signal decay is shown for selected regions of the calcaneus (top). A Cartesian high-resolution bSSFP scan is shown as a reference and as an indicator for bone density. The crosses represent the measurement points included in the seven TEs fit and the blank dots represent the measurement points that were included in the five TEs fit. Solid lines show the signal fitted with all TEs, dotted lines show the fitting with the latest five TEs. The cavum calcanei (ROI 1) has a high fat content and low trabecularization and minor differences using different TE regimes were visible. In ROI 2, a region with high trabecularization, signal deviation at the first TE compared to the fitted curve based on later TEs was observed. In the tuber calcanei (ROI 3, 4), characterized by lower fat content but also less trabecularized bone, signal deviations were visible

FIGURE 5 Multi-TE UTE acquisition results. Top image shows a Cartesian high resolution bSSFP scan of the ankle in a healthy volunteer. The PDFF and R_2^* maps originate from a 3D UTE stack-of-stars acquisition processed with either all available seven TEs (TE_{1-7}) or processed with only the later five TEs (TE_{3-7}). The white arrow highlights a region with higher bone density. In this high BV/TV region, R_2^* obtained with TE_{3-7} was larger than R_2^* obtained with TE_{1-7}. The difference in PDFF was smaller compared to R_2^* difference and the PDFF difference was ~4% in the region with high BV/TV area

healthy volunteers. The R_2^* maps including TE_1-TE_6, showed lower R_2^* values in regions with a higher BV/TV. Excluding the first echo (TE_{2-6}) increased the R_2^* in areas with a high BV/TV. Supporting Information Figure S1, which is available online, shows the comparison of R_2^* maps when the processing included either TE_{2-6} or TE_{2-7}. The difference maps using TE_{2-6} and TE_{2-7} showed no significant change in areas with high BV/TV.

To evaluate R_2^* and PDFF quantification errors in a clinical routine scan, Cartesian multi-GRE spine scans were

performed in three patients. Two patients suffered from metastasized cancer and showed osteoblastic changes in the spine (Figure 8 and Supporting Information Figure S2), resulting in increased bone density within the vertebral bodies. The acquired CT images showed typical osteoblastic lesions within multiple vertebral bodies. Due to the replacement of fatty marrow with calcified tissue, the average signal over echoes $\overline{S}$ showed low signal in the vertebral bodies. The signal decreased toward the anterior part as the subject was scanned without an anterior coil. The PDFF and the R_2^* map indicated pathological changes by presenting significantly reduced PDFF and increased R_2^* values. Supporting Information Figure S2 shows the mean

Cartesian bFFE [arb. u.]
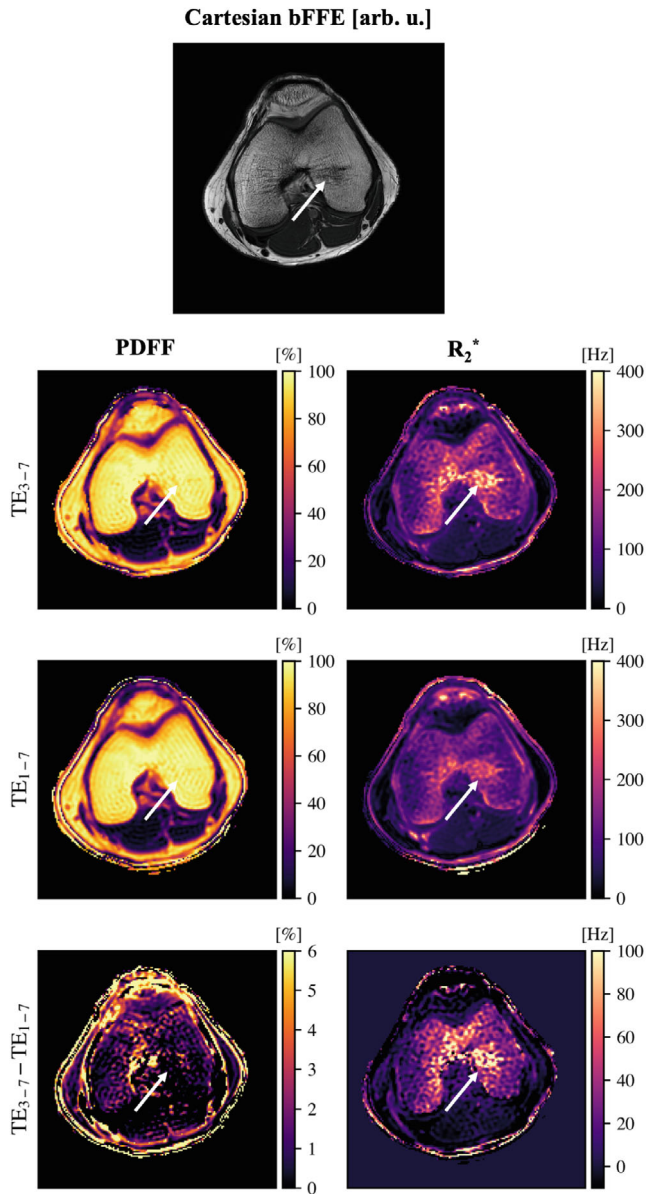
FIGURE 6 Multi-TE UTE acquisition results. Top image shows a Cartesian high resolution bSSFP scan of a healthy volunteer's knee. Multi-TE 3D UTE acquisition was performed to obtain PDFF and R_2^* maps which were processed with either all available seven TEs (TE_{1-7}) or processed with only the later five TEs (TE_{3-7}). In the difference maps areas with higher bone density showed higher differences of R_2^* values (indicated with white arrow)

signal decay in the specified ROIs. ROI L3, L4, and L5 had lower bone density, which was indicated by a higher signal amplitude at the first TE. There, the fit evaluated with the last five TEs was able to predict the first measurement point at TE = 1.12 ms. Regions with high trabecularization, T12 and L2, showed higher deviations of the signal at the first TE compared to the fit obtained from the last five TEs. The R_2^* difference maps (Figure 8) showed large differences in R_2^* and PDFF values within vertebrae

with higher BV/TV ratios (subjects 2 and 3). Specifically, the R_2^* difference maps show an underestimation of R_2^* including all TEs compared to R_2 determined by including only the last five TEs. For comparison, a patient with a PDFF in the healthy range and no calcified tissue changes is shown (subject 1). The BV/TV ratio was small compared to subjects 2 and 3, and the difference in R_2^* was neglectable.

4 | DISCUSSION

In this work, we addressed the feasibility of UTE imaging to measure the influence of local field inhomogeneities on the signal of trabecularized bone marrow at short TEs. Modern CSE-MRI relies on a water-fat model with a single exponential R_2^* decay aiming at the simultaneous extraction of R_2^* and PDFF. We showed that using such a water-fat model with a single exponential R_2^* decay results in R_2^* and PDFF bias in the static dephasing regime. The bias relates to a deviation of the signal decay from an exponential decay at short TEs. The signal decay at short TEs is Gaussian rather than exponential, and the deviation from the exponential decay increases in regions with higher trabecular bone density. Therefore, R_2^* can be underestimated when using short TEs in multi-echo GRE acquisitions of trabecularized bone marrow processed with a water-fat model with a single R_2^* decay, especially in regions with high bone density.

The present work relies on the characterization of the influence of local field inhomogeneities on the signal of trabecularized bone marrow using both simulations and in vivo UTE measurements. First, realistic simulations with masks generated from real trabecular bone structures were performed. The simulations showed that the deviation of the signal from the exponential signal decay was more prominent for a higher BV/TV ratio, which is in accordance with previous theoretical descriptions.[18,19] Second, UTE multi-TE measurements in the calcaneus and the knee reproduced in vivo the simulation-based predicted behavior. In areas with a higher BV/TV ratio, the difference between Gaussian and exponential decay was larger. The UTE multi-TE essentially enabled the experimental in vivo verification of the above result previously described primarily in theory and simulations.[17-19] Finally, the influence of a Gaussian decay on R_2^* and PDFF mapping was investigated in Cartesian scans for bone marrow CSE-MRI at 3T. We showed that the occurrence of the Gaussian decay in the presence of field inhomogeneities induces an R_2^* underestimation in trabecularized bone marrow regions when using CSE-based water fat separation with a single exponential R_2^* decay with a short TE. If a TE longer than 2 ms is used at 3T, we did not observe quantification
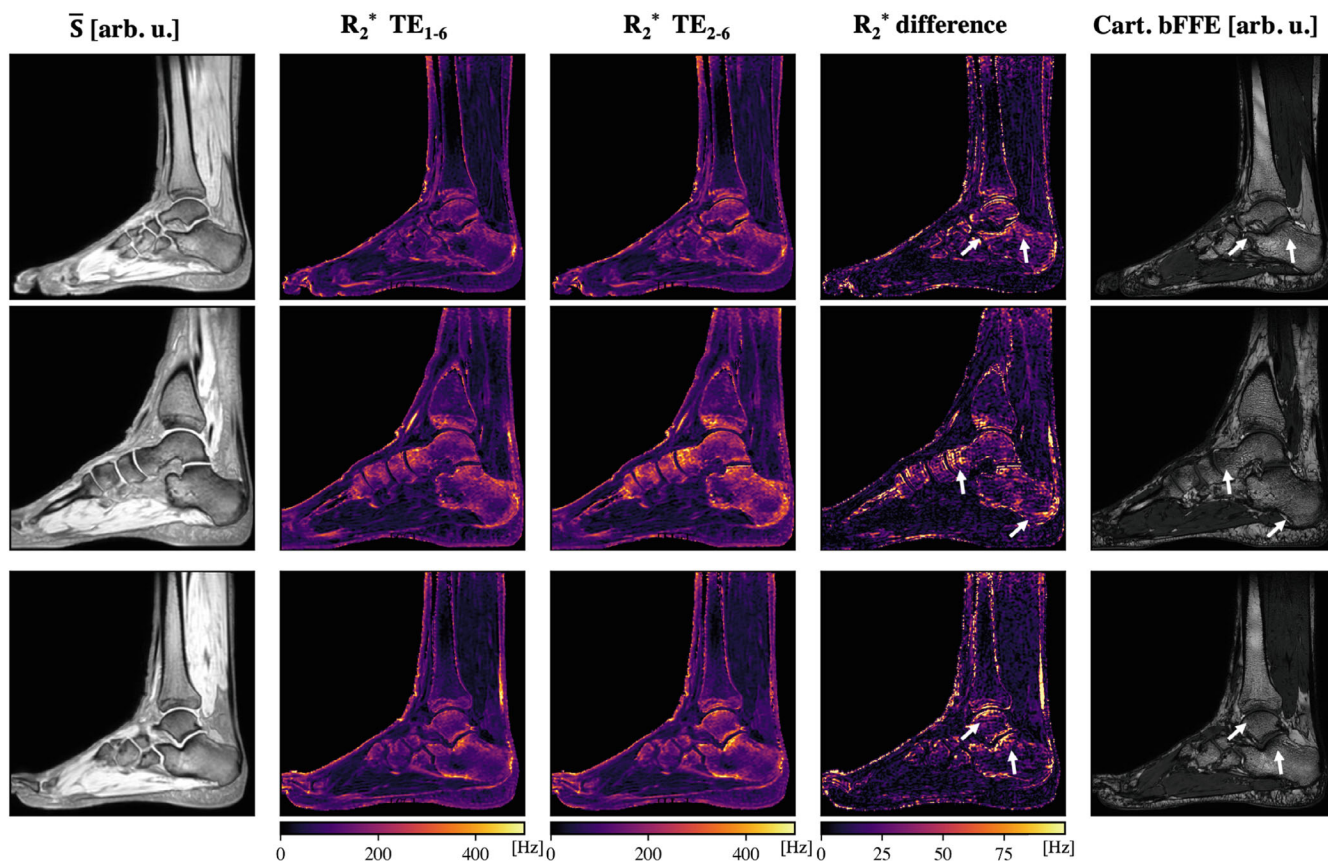
| $\overline{S}$ [arb. u.] | R_2^* TE$_{1-6}$ | R_2^* TE$_{2-6}$ | R_2^* difference | Cart. bFFE [arb. u.] |

FIGURE 7 Cartesian Dixon MR images and Cartesian high resolution bSSFP calcaneus scan images of three healthy volunteers. R_2^* maps were processed including the first echo TE$_{1-6}$ or excluding the first echo TE$_{2-6}$. The white arrows highlight areas with high BV/TV and larger R_2^* differences

errors, but if shorter TEs were used the static dephasing regime effect should be considered. When decreasing the minimum TE, the PDFF quantification errors were in general smaller than the R_2^* quantification errors. Consequently, from the results included in this study, we recommend a minimum first TE of 2 ms at 3T for CSE-MRI of trabecularized bone marrow especially in regions with high BV/TV. However, the critical time where Gaussian decay effects become significant needs further investigation for various anatomies and various scans that are used in the clinical routine or research setting.

The present UTE measurements were based on a multi-TE UTE acquisition employing a special sampling scheme. Specifically, each spoke was acquired multiple times where the TE was shifted in a random order to prevent the influence of eddy currents. A similar acquisition scheme has already been proposed for applications in the brain to study ultrashort T_2 components.[32] To the best of the authors' knowledge, the acquisition scheme has not yet been used and evaluated outside the brain. The present work uses the multi-UTE acquisition to experimentally verify the occurrence of the Gaussian signal decay in trabecularized bone marrow at short TEs. Such multi-UTE

acquisitions are associated with prolonged acquisition times, which might be difficult to adopt even in a research setting. However, the presented UTE results have two important implications. First, when using CSE-MRI to assess trabecularized bone marrow by performing simultaneous water-fat separation and R_2^* quantification with a water-fat model with a single exponential R_2^* decay, the minimum TE should be carefully selected such that the signal decay is exponential for the entire range of sampled TEs. Note, that the commonly used single exponential R_2^* decay signal model poorly describes the signal behavior at short TEs. Thus, each water-fat separation method[41–44] that relies on a single R_2^* exponential decay model underestimates R_2^* in areas with a distribution of local field inhomogeneities. Second, if the UTE signal of the trabecular bone matrix is of primary interest, the results suggest that UTE acquisitions combining fat and/or water suppression should be preferred, as described previously in.[45] At short TEs, the signal of the bone matrix becomes more significant, but the extraction of the bone matrix signal can be complicated further by the Gaussian decay of the bone marrow signal at short TEs, in the absence of fat suppression. However, additional work would be required
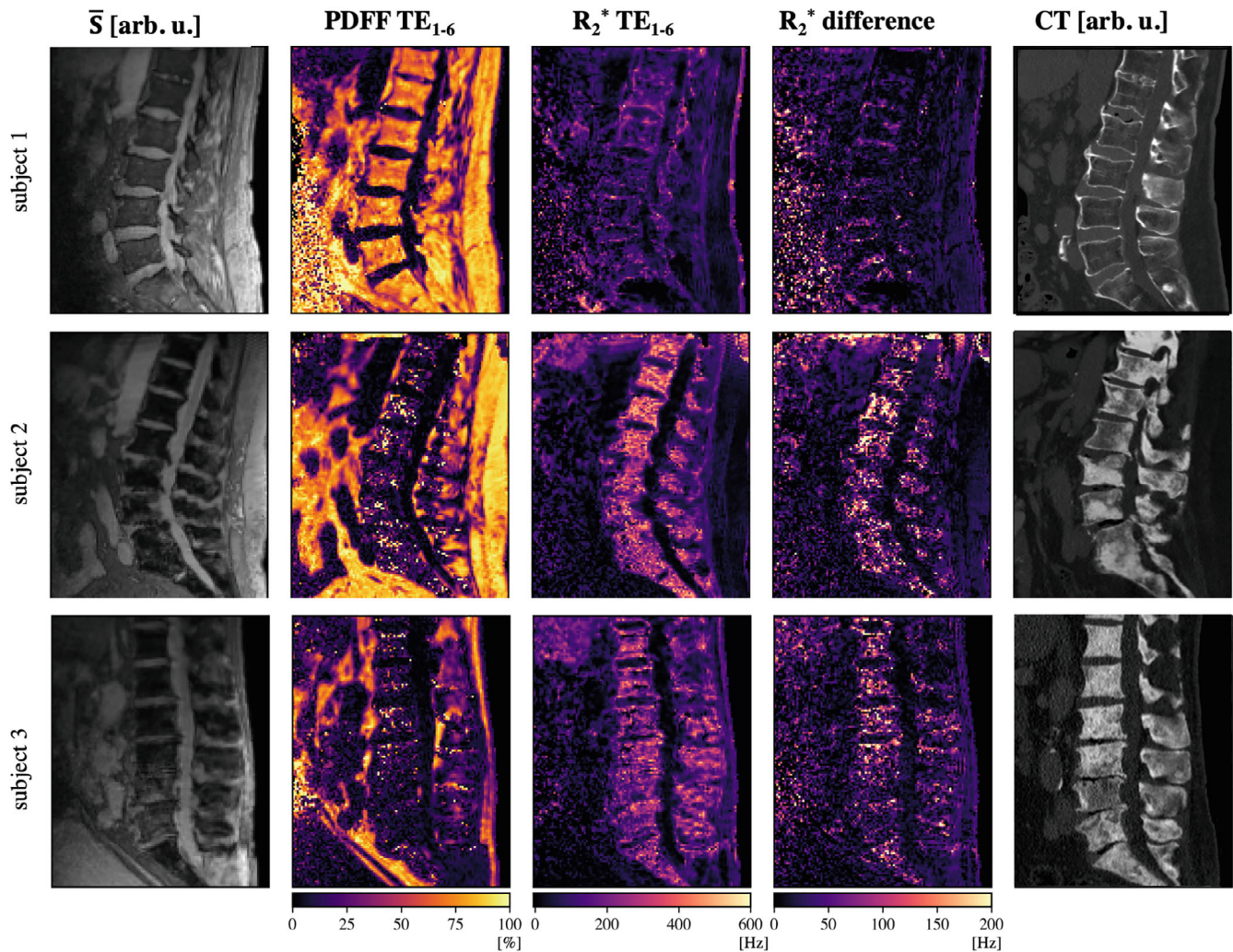
FIGURE 8 Cartesian Dixon MR images and CT images of the thoracolumbar spine of three patients (subject 1 suffered from a degenerative spine disease; subject 2 and subject 3 showed osteoblastic bone metastases. $\bar{S}$ shows the averaged signal over all echoes of the Cartesian multi-echo scan. Subject 1 showed a PDFF in the healthy range. In the patients with osteoblastic bone metastases, the fat fraction indicated pathological changes by showing significantly reduced fat fraction. The PDFF maps were obtained by including all TEs (TE_{1-6}). The R_2^* difference maps showed an underestimation of R_2^* including all six TEs (TE = 1.12 ms – 6.88 ms) compared to R_2^* determined by including only the last five TEs (TE = 2.08 ms – 6.88 ms). In subject 1, with PDFF values in the healthy range, the difference in R_2^* was neglectable. For subjects 1 and 2, a significant difference in R_2^* was visible in vertebrae with low PDFF and strong osteoblastic bone changes, meaning high BV/TV ratios

to investigate the impact of fat suppression on the signal decay at short TEs using either conventional fat saturation and selective water excitation techniques or recently proposed simultaneous fat-water excitation techniques.[46,47]

The single R_2^* signal model used for data post-processing was based on a model frequently used in the literature,[1] but this model relies on several simplifications such as no T1 bias correction and no multi-exponential R_2^*-decay effects. T1 bias has been most commonly minimized by the selection of a small flip angle.[38,39] R_2^* can in general be different between the water and fat components. A dual R_2^* fitting can improve accuracy in fat fraction estimation, but it reduces the precision

in fat quantification. Therefore, models with a single R_2^* fitting have been used[48,49] and good agreement has been reported in vivo between MRS-based and image-based PDFF.[48,50]

While the present study shows potential R_2^* and PDFF quantification errors with a water-fat model with a single exponential R_2^* decay in trabecularized bone marrow, it has relevant limitations. First, since bone contains roughly 30% free water protons and has a very short T_2^*, an increase in bone density also means a decrease in SNR. Due to the lower SNR, the relative error of the fit increases. Second, the influence of the local field distribution on the signal decay at short TE was small. The Gaussian decay effect

was visible only in areas where the BV/TV ratio drastically changed. Third, in red bone marrow regions, the signal decay can be further complicated. Red bone marrow is composed of both hematopoietic cells and fat cell.[1] The signal of each chemical component, such as water, lipids and proteins, decays with a different R_2^{*}[50] and the assumption of a single R_2^{*} signal model might fail. Fourth, neither fat deblurring nor T_2^{*} deblurring was performed in this study, which could further improve image quality especially for the scans with higher resolution.[51] However, while image quality and resolution improve with deblurring methods, the ROI-based analysis should not be affected. Fifth, in this study two clinical scans were included which showed osteoblastic bone metastases. Additional subjects would be required to investigate further the exact range of quantification errors for various clinically relevant scans. Furthermore, additional work would be required to investigate the critical time and a signal model that describes the signal decay at short and long TEs in the presence of strong local field inhomogeneities.

5 | CONCLUSIONS

We showed with the help of simulations and UTE measurements that due to a distribution of local field inhomogeneities in trabecularized bone marrow regions R_2^{*} is underestimated when using a water-fat model with an exponential R_2^{*} decay model at short TEs. The bias relates to a Gaussian signal decay instead of an exponential decay at short TEs. R_2^{*} can be underestimated when using short TEs, shorter than 2 ms at 3 T, in multi-echo GRE acquisitions of trabecularized bone marrow, especially in regions with high bone density.

DATA AVAILABILITY STATEMENT
Example Python code of our implementation on trabecular bone simulations will be made freely available for download at https://github.com/BMRRgroup/trabecular_bone_sim. Example MATLAB code for graph-cut field-mapping from[40] is freely available at https://github.com/BMRRgroup/fieldmapping-graph-cut. Example MATLAB code to solve for chemical species separation (CSS) as described in[37] is freely available for download at https://github.com/BMRRgroup/MRI_field_contributions.

ORCID
Sophia Kronthaler https://orcid.org/0000-0001-7913-1238
Maximilian N. Diefenbach https://orcid.org/0000-0002-5581-885X
Christof Boehm https://orcid.org/0000-0003-1321-5804

REFERENCES
1. Karampinos DC, Ruschke S, Dieckmeyer M, et al. Quantitative MRI and spectroscopy of bone marrow. *J Magn Reson Imaging*. 2018;47:332-353.
2. Sollmann N, Löffler MT, Kronthaler S, et al. MRI-based quantitative osteoporosis imaging at the spine and femur. *J Magn Reson Imaging*. 2021;54:12-35.
3. Chang G, Boone S, Martel D, et al. MRI assessment of bone structure and microarchitecture. *J Magn Reson Imaging*. 2017;46:323-337.
4. Burr DB, Allen MR. *Basic and Applied Bone Biology*. 2nd ed. Academic Press; 2019.
5. Wehrli FW, Song HK, Saha PK, Wright AC. Quantitative MRI for the assessment of bone structure and function. *NMR Biomed*. 2006;19:731-764.
6. Chung H, Wehrli FW, Williams JL, Kugelmass SD. Relationship between NMR transverse relaxation, trabecular bone architecture, and strength. *Proc Natl Acad Sci USA*. 1993;90:10250-10254.
7. Majumdar S, Thomasson D, Shimakawa A, Genant HK. Quantitation of the susceptibility difference between trabecular bone and bone marrow: experimental studies. *Magn Reson Med*. 1991;22:111-127.
8. Wehrli FW, Ford JC, Attie M, Kressel HY, Kaplan FS. Trabecular structure: preliminary application of MR interferometry. *Radiology*. 1991;179:615-621.
9. Diefenbach MN, Meineke J, Ruschke S, Baum T, Gersing A, Karampinos DC. On the sensitivity of quantitative susceptibility mapping for measuring trabecular bone density. *Magn Reson Med*. 2019;81:1739-1754.
10. Wu HZ, Zhang XF, Han SM, et al. Correlation of bone mineral density with MRI T2* values in quantitative analysis of lumbar osteoporosis. *Arch Osteoporos*. 2020;15:18.
11. Gao Y, Wang O, Guan W, et al. Bone mineral density and trabecular bone score in patients with 21-hydroxylase deficiency after glucocorticoid treatment. *Clin Endocrinol (Oxf)*. 2021;94:765-773.
12. Kuhn JP, Hernando D, Meffert PJ, et al. Proton-density fat fraction and simultaneous R2* estimation as an MRI tool for assessment of osteoporosis. *Eur Radiol*. 2013;23:3432-3439.
13. Griffith JF, Yeung DK, Antonio GE, et al. Vertebral bone mineral density, marrow perfusion, and fat content in healthy men and men with osteoporosis: dynamic contrast-enhanced MR imaging and MR spectroscopy. *Radiology*. 2005;236:945-951.
14. Baum T, Yap SP, Dieckmeyer M, et al. Assessment of whole spine vertebral bone marrow fat using chemical shift-encoding based water-fat MRI. *J Magn Reson Imaging*. 2015;42:1018-1023.

15. Schmeel FC, Luetkens JA, Feißt A, et al. Quantitative evaluation of T2* relaxation times for the differentiation of acute benign and malignant vertebral body fractures. *Eur J Radiol.* 2018;108:59-65.

16. Majumdar S. Quantitative study of the susceptibility difference between trabecular bone and bone marrow: computer simulations. *Magn Reson Med.* 1991;22:101-110.

17. Ford JC, Wehrli FW, Chung H-W. Magnetic field distribution in models of trabecular bone. *Magn Reson Med.* 1993;30:373-379.

18. Yablonskiy DA. Quantitation of intrinsic magnetic susceptibility-related effects in a tissue matrix. *Phantom Study Magn Reson Med.* 1998;39:417-428.

19. Yablonskiy DA, Haacke EM. Theory of NMR signal behavior in magnetically inhomogeneous tissues: the static dephasing regime. *Magn Reson Med.* 1994;32:749-763.

20. Liang ZP, Lauterbur PC. *Principles of magnetic resonance imaging: a signal processing perspective.* SPIE Optical Engineering Press; 2000.

21. Song HK, Wehrli FW, Ma J. Field strength and angle dependence of trabecular bone marrow transverse relaxation in the calcaneus. *J Magn Reson Imaging.* 1997;7:382-388.

22. Ganter C. Static susceptibility effects in balanced SSFP sequences. *Magn Reson Med.* 2006;56:687-691.

23. Storey P, Novikov DS. Signatures of microstructure in R2* decay: defining the limits of the weak field approximation. *In Proceedings of the 29th Scientific Meeting of ISMRM, Virtual Conference*; 2020:3248.

24. Martel D, Leporq B, Bruno M, Regatte RR, Honig S, Chang G. Chemical shift-encoded MRI for assessment of bone marrow adipose tissue fat composition: pilot study in premenopausal versus postmenopausal women. *Magn Reson Imaging.* 2018;53:148-155.

25. Sharma SD, Artz NS, Hernando D, Horng DE, Reeder SB. Improving chemical shift encoded water-fat separation using object-based information of the magnetic field inhomogeneity. *Magn Reson Med.* 2015;73:597-604.

26. Koch KM, Papademetris X, Rothman DL, Graaf RAD. Rapid calculations of susceptibility-induced magnetostatic field perturbations forin vivo magnetic resonance. *Phys Med Biol.* 2006;51:6381-6402.

27. Ruschke S, Syväri J, Dieckmeyer M, et al. Physiological variation of the vertebral bone marrow water T2 relaxation time. *NMR Biomed.* 2021;34:e 4439.

28. Dieckmeyer M, Ruschke S, Cordes C, et al. The need for T_2 correction on MRS-based vertebral bone marrow fat quantification: implications for bone marrow fat fraction age dependence. *NMR Biomed.* 2015;28:432-439.

29. Ren J, Dimitrov I, Sherry AD, Malloy CR. Composition of adipose tissue and marrow fat in humans by 1H NMR at 7 tesla. *J Lipid Res.* 2008;49:2055-2062.

30. Weiger M, Pruessmann KP. Short-T2 MRI: principles and recent advances. *Prog Nucl Magn Reson Spectrosc.* 2019;114-115:237-270.

31. Qian Y, Boada FE. Acquisition-weighted stack of spirals for fast high-resolution three-dimensional ultra-short echo time MR imaging. *Magn Reson Med.* 2008;60:135-145.

32. Boucneau T, Cao P, Tang S, et al. In vivo characterization of brain ultrashort-T2 components. *Magn Reson Med.* 2018;80:726-735.

33. Ruschke S, Eggers H, Kooijman H, et al. Correction of phase errors in quantitative water-fat imaging using a monopolar time-interleaved multi-echo gradient echo sequence. *Magn Reson Med.* 2017;78:984-996.

34. Kronthaler S, Rahmer J, Bornert P, et al. Trajectory correction based on the gradient impulse response function improves high-resolution UTE imaging of the musculoskeletal system. *Magn Reson Med.* 2021;85:2001-2015.

35. Yu H, Shimakawa A, McKenzie CA, Brodsky E, Brittain JH, Reeder SB. Multiecho water-fat separation and simultaneous R2* estimation with multifrequency fat spectrum modeling. *Magn Reson Med.* 2008;60:1122-1134.

36. Bydder M, Yokoo T, Hamilton G, et al. Relaxation effects in the quantification of fat using gradient echo imaging. *Magn Reson Imaging.* 2008;26:347-359.

37. Diefenbach MN, Liu C, Karampinos DC. Generalized parameter estimation in multi-echo gradient-echo-based chemical species separation. *Quant Imaging Med Surg.* 2020;10:554-567.

38. Karampinos DC, Yu H, Shimakawa A, Link TM, Majumdar S. T1-corrected fat quantification using chemical shift-based water/fat separation: application to skeletal muscle. *Magn Reson Med.* 2011;66:1312-1326.

39. Liu C-Y, McKenzie CA, Yu H, Brittain JH, Reeder SB. Fat quantification with IDEAL gradient echo imaging: correction of bias from T1 and noise. *Magn Reson Med.* 2007;58:354-364.

40. Boehm C, Diefenbach MN, Makowski MR, Karampinos DC. Improved body quantitative susceptibility mapping by using a variable-layer single-min-cut graph-cut for field-mapping. *Magn Reson Med.* 2021;85:1697-1712.

41. Hernando D, Haldar JP, Sutton BP, Ma J, Kellman P, Liang Z-P. Joint estimation of water/fat images and field inhomogeneity map. *Magn Reson Med.* 2008;59:571-580.

42. Reeder SB, Pineda AR, Wen Z, et al. Iterative decomposition of water and fat with echo asymmetry and least-squares estimation (IDEAL): application with fast spin-echo imaging. *Magn Reson Med.* 2005;54:636-644.

43. Hernando D, Kellman P, Haldar JP, Liang Z-P. Robust water/fat separation in the presence of large field inhomogeneities using a graph cut algorithm. *Magn Reson Med.* 2010;63:79-90.

44. Dong J, Liu T, Chen F, et al. Simultaneous phase unwrapping and removal of chemical shift (SPURS) using graph cuts: application in quantitative susceptibility mapping. *IEEE Trans Med Imaging.* 2015;34:531-540.

45. Ma YJ, Chen Y, Li L, et al. Trabecular bone imaging using a 3D adiabatic inversion recovery prepared ultrashort TE cones sequence at 3T. *Magn Reson Med.* 2020;83:1640-1651.

46. Liu J, Christiansen SD, Drangova M. Single multi-echo GRE acquisition with short and long echo spacing for simultaneous quantitative mapping of fat fraction, B0 inhomogeneity, and susceptibility. *Neuroimage.* 2018;172:703-717.

47. Bachrata B, Strasser B, Bogner W, et al. Simultaneous multiple resonance frequency imaging (SMURF): fat-water imaging using multi-band principles. *Magn Reson Med.* 2021;85:1379-1396.

48. Karampinos DC, Melkus G, Baum T, Bauer JS, Rummeny EJ, Krug R. Bone marrow fat quantification in the presence of trabecular bone: initial comparison between water-fat imaging and single-voxel MRS. *Magn Reson Med.* 2014;71:1158-1165.

49. Li G, Xu Z, Gu H, et al. Comparison of chemical shift-encoded water–fat MRI and MR spectroscopy in quantification of marrow fat in postmenopausal females. *J Magn Reson Imaging*. 2017;45:66-73.

50. Karampinos DC, Ruschke S, Dieckmeyer M, et al. Modeling of T2* decay in vertebral bone marrow fat quantification. *NMR Biomed*. 2015;28:1535-1542.

51. Wang K, Yu H, Brittain JH, Reeder SB, Du J. K-space water-fat decomposition with T2* estimation and multifrequency fat spectrum modeling for ultrashort echo time imaging. *J Magn Reson Imaging*. 2010;31:1027-1034.

SUPPORTING INFORMATION

Additional supporting information may be found in the online version of the article at the publisher's website.

Figure S1 The same Dixon MR images and Cartesian high resolution bSSFP calcaneus scan as shown in Figure 7. R_2^* maps were processed using either 6 or 7 echoes. In both cases the first echo was excluded. In areas with high BV/TV (white arrows) no significant R_2^* differences were observed.

Figure S2 CT and Cartesian Dixon MR images of the thoracolumbar spine of a patient with osteoblastic bone metastases. The fat fraction and the R_2^* map indicate pathological changes by showing significantly reduced fat fraction and elevated R_2^*-values, respectively. In the right column signal decay curves for regions within specific vertebrae are shown. The fit including all 6 TEs (TE = 1.12 ms – 6.88 ms) deviated from the fit based on the last 5 TEs (TE = 2.08 ms – 6.88 ms). The deviation was largest for the first measurement point at TE = 1.12 ms and in regions with high trabecularization (T12 and L2).